Engineering Analysis with Boundary Elements 171 (2025) 106090

Contents lists available at ScienceDirect

Engineering Analysis with Boundary Elements

journal homepage: www.elsevier.com/locate/enganabound

Phase-field modeling for curvature-dependent tissue growth on surfaces

Soobin Kwak [a], Yongho Choi [b], Jian Wang [c], Yunjae Nam [d], Junseok Kim [a,*]

[a] Department of Mathematics, Korea University, Seoul, 02841, Republic of Korea
[b] Department of Computer & Information Engineering, Daegu University, Gyeongsan-si, Gyeongsangbuk-do, 38453, Republic of Korea
[c] School of Mathematics and Statistics, Nanjing University of Information Science and Technology, Nanjing, 210044, China
[d] Program in Actuarial Science and Financial Engineering, Korea University, Seoul, 02841, Republic of Korea

ARTICLE INFO

MSC:
65M06
65M55
74S20

Keywords:
Modified Allen–Cahn equation
Curvature-dependent tissue growth
Surface limited tissue growth
Phase-field model

ABSTRACT

We propose a novel phase-field model for simulating curvature-dependent and surface-limited tissue growth on curved surfaces. The proposed mathematical model consists of a modified Allen–Cahn (AC) equation with a non-standard variable mobility and a growth term that depends on curvature and surface limitations. To solve the equations numerically, we use an operator splitting technique. We split the governing equation into a modified AC equation, and curvature-dependent and surface limited growth equation. To validate the high performance of the proposed mathematical model in realistic simulations, we conduct several numerical simulations such as those with synthetic conditions and comparisons with real experimental data. The computational results demonstrate the robustness and efficiency of the new phase-field model in accurately capturing realistic tissue growth phenomena on curved surfaces.

1. Introduction

The development of mathematical models for tissue growth is very important for understanding complex biological processes and the advancement of effective medical interventions. The process of tissue growth is governed by a complex interplay of factors such as gradients of mechanical stresses [1], initial cell seeding [2], mechanical stimuli [3], and biochemical signaling pathways [4]. These elements are often difficult to examine experimentally due to their complexity and the large scale at which they operate. Mathematical modeling provides a systematic framework to analyze these diverse factors. Predictive modeling allows researchers to simulate tissue development across different conditions and provides a valuable opportunity to investigate scenarios that are otherwise difficult to replicate in the laboratory. Such modeling is essential for gaining deeper insights into advances in fields such as tissue engineering techniques [5,6]. Furthermore, these models are necessary for hypothesis testing and identifying key factors that affect tissue growth. They help to refine experimental designs and potentially reduce the reliance on extensive animal testing. In medical applications, these models can help optimize the design of scaffolds for tissue regeneration [7,8]. Ultimately, mathematical modeling is an indispensable tool in bridging the gap between theoretical biology and clinical practice, and it facilitates the development of innovative solutions in regenerative medicine and other biomedical fields.

Therefore, many researchers have actively conducted studies on tissue growth using mathematical models. Huang et al. [9] conducted a study on a mathematical model that simulates the growth of prostate cancer and the effects of drugs. They proposed a second-order numerical method to solve this model, which is represented by a phase-field system. Alotaibi et al. [10] studied a breast tumor growth model using a finite volume method. The presented mathematical model consists of a system of ordinary differential equations and partial differential equations, modeling the development of breast cancer. López-Agredo et al. [11] considered a mathematical model of tumor growth in the brain. The proposed system includes a nonlinear term that describes chemoattraction. Han et al. [12] studied a tumor growth model under immune surveillance using a differential equation derived from a catalytic Michaelis–Menten reaction. Using unified colored noise and small delay approximations, The study examined how time-delay and noise intensity in non-Gaussian colored noise influence transitions between tumor and tumor-free states, highlighting the dominant role of noise intensity in altering the most probable trajectories. Ghanizadeh et al. [13] investigated the dynamics of the immune system and cancer using mathematical modeling, particularly focusing on immunoediting through a system of two differential equations to analyze tumor fate across three main phases. Wang et al. [14] presented a mathematical model of tumor-immune interactions that focuses on estrogen's role in

* Corresponding author.
E-mail address: cfdkim@korea.ac.kr (J. Kim).
URL: https://mathematicians.korea.ac.kr/cfdkim/ (J. Kim).

https://doi.org/10.1016/j.enganabound.2024.106090
Received 28 October 2024; Received in revised form 11 December 2024; Accepted 19 December 2024
Available online 27 December 2024

cancer. The model uses Lyapunov stability analysis and AI-MCMC for parameter evaluation and uncertainty assessment.

Numerous studies emphasize the role of curvature in the mathematical modeling of tissue growth. In [15], the authors explore how substrate geometry affects tissue growth in vitro. As shown in Fig. 1, tissue growth varies with the curvature of the interface. They emphasize that geometric structures play a critical role in both tissue growth and bone remodeling processes.

As confirmed by the in vitro experimental result in Fig. 1, tissue grows even when the curvature is less than 0. However, in [16], the tissue was modeled not to grow when the curvature is less than 0. To overcome this limitation, we propose a new phase-field model where the tissue growth rate varies with the curvature.

The primary objective of this article is to propose a novel phase-field equation for curvature-dependent and surface-limited tissue growth on curved surfaces. The proposed mathematical model, based on a modified Allen–Cahn (AC) equation with variable mobility and curvature-dependent, surface-limited growth, is solved numerically using an operator splitting method. Numerical simulations, including synthetic and experimental comparisons, demonstrate the model's robustness and efficiency in capturing realistic tissue growth on curved surfaces.

The structure of this article is organized as follows. Section 2 presents the proposed phase-field model for tissue growth that is curvature-dependent and surface-limited on curved surfaces. Section 3 discusses the numerical methods and test results. Finally, Section 4 provides the conclusion.

2. Mathematical model

We present the proposed mathematical model for tissue growth on a curved surface. We begin with a single layer of cells on a curved surface, highlighted in red in Fig. 2(a), and allow the cells to grow in a direction perpendicular to the surface. Here, the gray region represents the substrate and the white area shows the growth region where cells can grow. From the growth region perspective, the convex curve is the black dashed line, and the concave curve is the blue solid line in Fig. 2(a). In the convex region, the cells overlap, while in the concave region, the cells are rarefied. Because the cells cannot physically overlap each other, they push against each other and stack up in the convex region, while in the concave region, they adhere to one another, stick together, and settle down, resulting in an effectively thinner layer of cells, as shown in Fig. 2(b). We model this uneven cell growth by relating it to curvature of the surface. The surface curvature is shown as arrows in Fig. 2(b). The curvature is assigned a sign based on the surface geometry, with convex regions having positive curvature and concave regions having negative curvature. We add some constant growth rate in the direction of growth on the surface. Then, the resulting direction of cell growth is shown in Fig. 2(c) and the arrows show both the direction and magnitude of the growth. Fig. 2(d) illustrates the position of the interface after cell growth.

The proposed phase-field model for curvature-dependent and surface-limited tissue growth on curved surfaces is given as

$$\phi_t(\mathbf{x},t) = M(\phi(\mathbf{x},t))\left[-\frac{F'(\phi(\mathbf{x},t))}{\epsilon^2} + \Delta\phi(\mathbf{x},t)\right] + KSG(\phi(\mathbf{x},t)), \mathbf{x}\in\Omega,\ t>0, \tag{1}$$

where $\phi(\mathbf{x},t)$ is a normalized density at position $\mathbf{x}$ and time t, ϵ is a positive coefficient related to the thickness of the interfacial transition layer, $M(\phi) = 4(\phi-0.5)^2$ is a non-standard phase-dependent mobility, which preserves interface position of tissue [17], see Fig. 3(a), and $F(\phi) = 0.25\phi^2(\phi-1)^2$, which is a double-well potential [18] having two minima: $\phi = 0$ is the empty region and $\phi = 1$ represents the tissue region, including the substrates. Unlike the classical variable mobility approach [19,20], we use a non-standard, phase-dependent mobility, which keeps the interface location ($\phi \approx 0.5$) where the mobility is close to zero, $M(\phi) \approx 0$. This choice is motivated by the need to model the tissue growth phenomenon in a way that allows the tissue interfaces to grow according to the growth term, while maintaining a smooth interfacial transition layer, such as a hyperbolic transition layer. Simultaneously, this approach minimizes the motion of the interface driven by mean curvature, which is an intrinsic property of the AC equation [21].

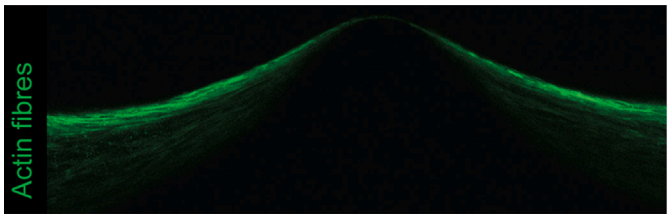

Fig. 1. Reprinted from Bidan et al. [15] with permission from PLOS ONE.

As schematically illustrated in Fig. 2, tissue growth occurs more rapidly in convex regions and at a slower rate in concave regions. Based on this observation, we propose a curvature-dependent, surface-limited tissue growth model as follows:

$$KSG(\phi(\mathbf{x},t)) = \lambda(\phi(\mathbf{x},t))[1+\alpha\tanh(\beta(\phi(\mathbf{x},t))\kappa(\phi(\mathbf{x},t)))], \tag{2}$$

where

$$\lambda(\phi(\mathbf{x},t)) = \lambda_0\phi(\mathbf{x},t)(1-\phi(\mathbf{x},t)) \quad \text{and} \quad \beta(\phi(\mathbf{x},t)) = \beta_0\phi(\mathbf{x},t)(1-\phi(\mathbf{x},t))$$

account for surface-limited tissue growth. Here, λ_0 and β_0 are growth and scaling constant parameters, and $\kappa(\phi) = \nabla\cdot(\nabla\phi/|\nabla\phi|)$ is the curvature of the interface, the coefficient, $0 \le \alpha \le 1$, represents the magnitude of the curvature effect, see Fig. 3(b) for the values of $[1+\alpha\tanh(\beta\kappa)]$ plotted against κ. The homogeneous Neumann boundary conditions are used.

3. Numerical method and tests

3.1. Computational solution algorithm

Now, let us split Eq. (1) as follows:

$$\phi_t(\mathbf{x},t) = M(\phi(\mathbf{x},t))\left[-\frac{F'(\phi(\mathbf{x},t))}{\epsilon^2} + \Delta\phi(\mathbf{x},t)\right], \tag{3}$$

$$\phi_t(\mathbf{x},t) = \lambda(\phi(\mathbf{x},t))[1+\alpha\tanh(\beta(\phi(\mathbf{x},t))\kappa(\phi(\mathbf{x},t)))], \tag{4}$$

Let $\Omega = (L_x,R_x)\times(L_y,R_y)$ be the computational domain in two-dimensional space and $\Omega_h = \{(x_i,y_j)|x_i = L_x + h(i-0.5),\ y_j = L_y + h(j-0.5),\ 1\le i\le N_x,\ 1\le j\le N_y\}$ be its discretized domain with the uniform spatial mesh h. Let $\phi_{ij}^n = \phi(x_i,y_j,n\Delta t)$. We use the operator splitting method [23]. As the first step, we compute Eq. (3) by applying the Euler's scheme with the known value ϕ^n:

$$\frac{\phi_{ij}^* - \phi_{ij}^n}{\Delta t} = M(\phi_{ij}^n)\left[-\frac{F'(\phi_{ij}^n)}{\epsilon^2} + \Delta_d\phi_{ij}^n\right], \tag{5}$$

where $\Delta_d\phi_{ij}$ is the standard five-point discrete Laplacian operator with

$$\phi_{0j} = \phi_{1j},\quad \phi_{N_x+1,j} = \phi_{N_xj},\quad \phi_{i0} = \phi_{i1},\quad \phi_{i,N_y+1} = \phi_{iN_y}.$$

Eq. (5) can be rewritten as

$$\phi_{ij}^* = \phi_{ij}^n + \Delta t M(\phi_{ij}^n)\left[-\frac{F'(\phi_{ij}^n)}{\epsilon^2} + \Delta_d\phi_{ij}^n\right],\ \text{for } (x_i,y_j)\in\Omega_h, \tag{6}$$

The solution of Eq. (4) is obtained using the frozen coefficient technique as follows:

$$\phi_{ij}^{n+1} = \frac{\phi_{ij}^*}{\phi_{ij}^* + (1-\phi_{ij}^*)e^{-\lambda_0\Delta t[1+\alpha\tanh(\beta_{ij}^*\kappa_{ij}^*)]}}. \tag{7}$$

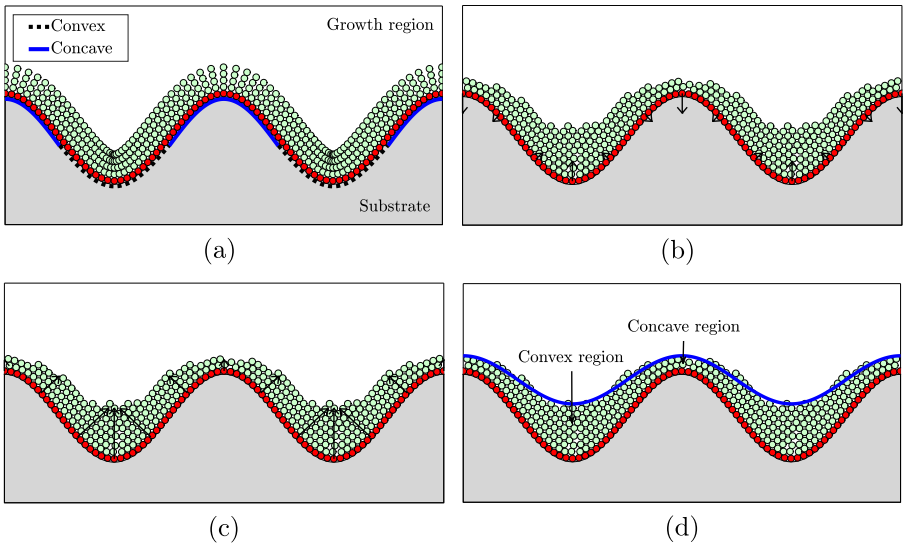

Fig. 2. Illustration of the proposed model for cell growth on a curved surface. (a) Initial single layer of cells (in red) growing perpendicular to the curved surface. The gray area represents the substrate and the white area shows the growth region where cells can grow. (b) Cells stack in convex regions and spread out in concave regions due to curvature effects. Arrows indicate the curvature at different points on the surface. (c) Arrows represent the direction and magnitude of adjusted cell growth, showing the uneven growth behavior. (d) Final interface position of the cells after growth.

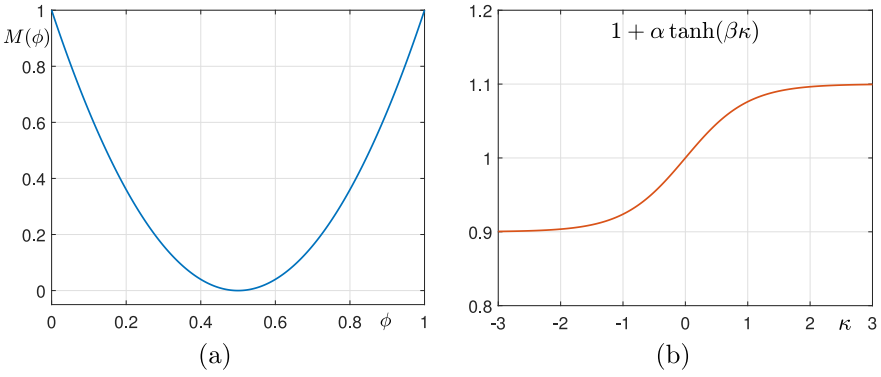

Fig. 3. (a) Schematic representation of the non-standard phase-dependent mobility $M(\phi) = 4(\phi - 0.5)^2$. (b) Plot of $[1 + \alpha\tanh(\beta\kappa)]$ against κ with $\alpha = 0.1$, and $\beta(\phi) = \beta_0$, where $\beta_0 = 1$.

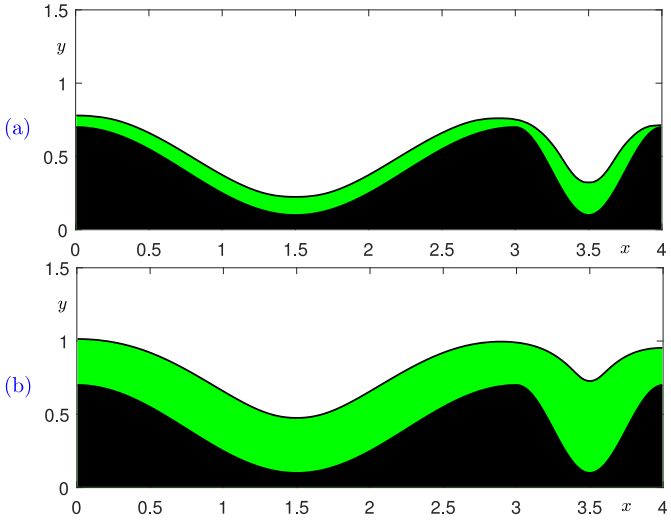

Fig. 4. Effect of λ_0 on the temporal evolution of ϕ for (a) $\lambda_0 = 30$ and (b) $\lambda_0 = 100$.

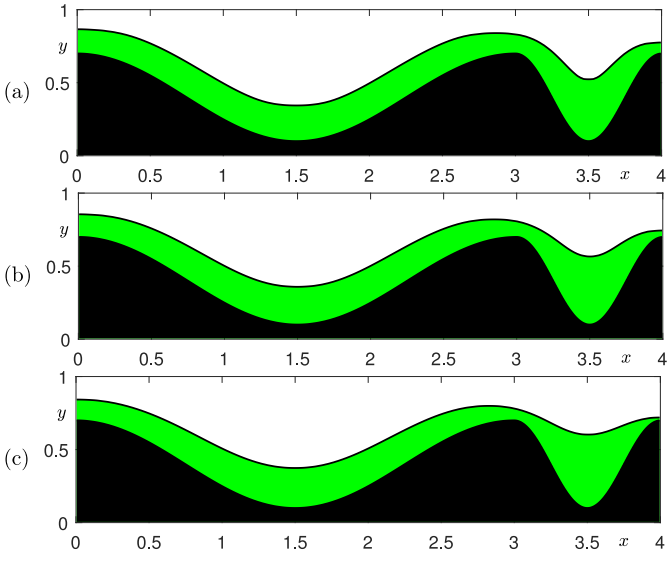

Fig. 5. Effect of α on the temporal evolution of ϕ with (a) $\alpha = 0.05$, (b) $\alpha = 0.5$, and (c) $\alpha = 1$.

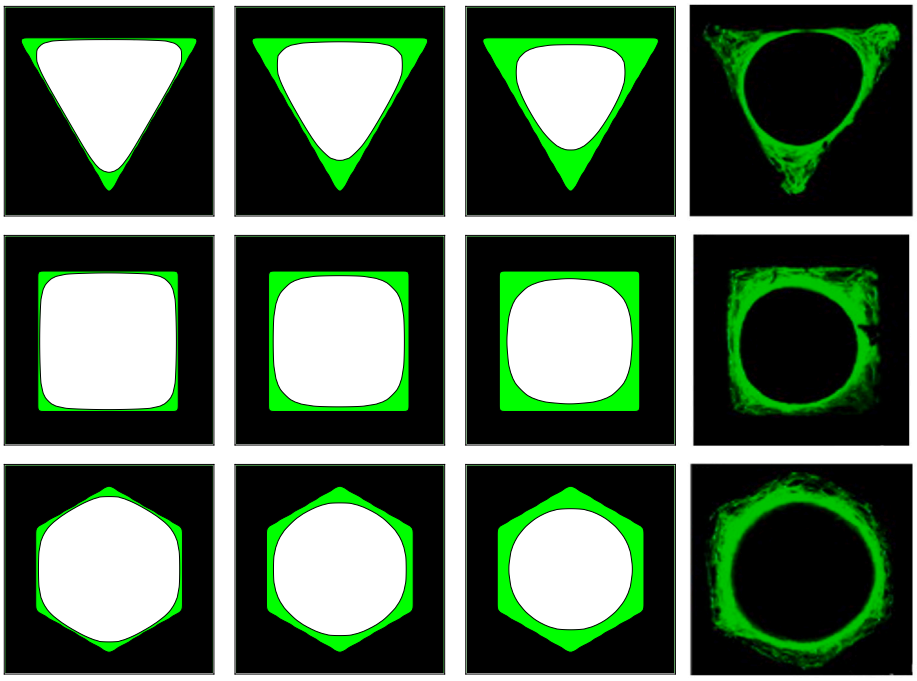

Fig. 6. The first column is the result of evolution for $t = 10\,000\Delta t$ on different scaffolds. The second column is the result of evolution for $t = 20\,000\Delta t$ on different scaffolds. The third column is the result of evolution for $t = 30\,000\Delta t$ on different scaffolds. The fourth column is reprinted from Rumpler et al. [22].

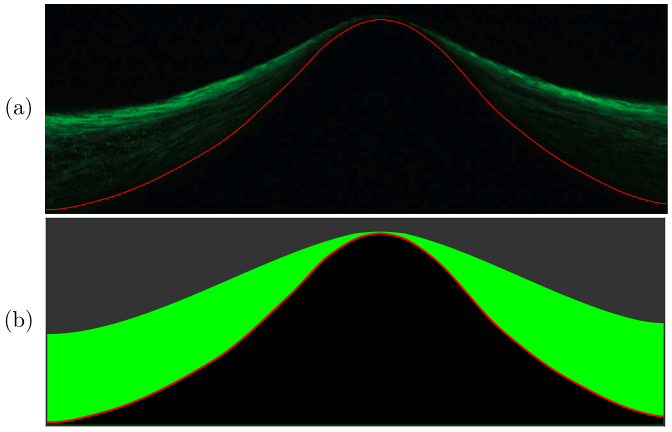

Fig. 7. (a) Reprinted from Bidan et al. [15] with permission from PLOS ONE. (b) Result of the proposed model.

For the stability of the proposed computational scheme is as follows. In the first step, if the time step satisfies $\Delta t \le 4\epsilon^2 h^2/(h^2 + 16\epsilon^2)$, then Eq. (6) is stable [24]. In the second step, Eq. (7) is unconditionally stable. Therefore, if $\Delta t \le 4\epsilon^2 h^2/(h^2 + 16\epsilon^2)$, then the overall numerical solution is stable.

3.2. Computational tests

3.2.1. Convergence test

Let us set an initial condition

$$\phi(x, y, 0) = \frac{1}{2}\left[1 + \tanh\left(\frac{0.5 - y + 0.1\cos(2\pi x)}{2\sqrt{2}\epsilon}\right)\right], \quad (x, y) \in \Omega \tag{8}$$

where $\Omega = (0, 1) \times (0, 1)$. We define the convergence error as following:

$$err_{h/\frac{h}{2}} = \sqrt{\frac{1}{N_x}\frac{1}{N_y}\sum_{i=1}^{N_x}\sum_{j=1}^{N_y}\left(\phi_{h_{ij}} - \frac{\phi_{\frac{h}{2}2i,2j} + \phi_{\frac{h}{2}2i-1,2j} + \phi_{\frac{h}{2}2i,2j-1} + \phi_{\frac{h}{2}2i-1,2j-1}}{4}\right)^2}.$$

Table 1
The convergence error and rate.

$(h, \Delta t)$	$(2^{-5}, \Delta t_{\max})$	Rate	$(2^{-6}, \Delta t_{\max}/4)$	rate	$(2^{-7}, \Delta t_{\max}/4^2)$
$err_{h/\frac{h}{2}}$	1.9620e−03	1.90	5.2752e−04	1.99	1.3265e−04

The convergence rate is defined as $\log_2(err_{h/\frac{h}{2}}/err_{\frac{h}{2}/\frac{h}{4}})$. To investigate the convergence, the following parameters are used $h_{\max} = 2^{-5}$, $h_{\min} = 2^{-8}$, $\epsilon = 8h_{\max}/(4\sqrt{2}\tanh^{-1}(0.9))$, $\Delta t_{\max} = 4\epsilon^2 h_{\max}^2/(h_{\max}^2 + 16\epsilon^2)$, total time $T = 100\Delta t_{\max}$, $\alpha = 0.1$, $\beta_0 = 0.1$, and $\lambda_0 = 10$.

As shown in Table 1, the method is confirmed to have second-order accuracy in space and first-order accuracy in time.

3.2.2. Effect of λ_0

We investigate the effect of the tissue growth parameter λ_0 using the parameters $\epsilon = \epsilon_5$, $h = 0.01$, $\Delta t = 4\epsilon^2 h^2/(h^2 + 16\epsilon^2)$, $T = 20\,000\Delta t$, $\alpha = 0.5$, and $\beta_0 = 0.1$, with the initial condition

$$\phi(x, y, 0) = \begin{cases} \frac{1}{2} + \frac{1}{2}\tanh\left(\frac{0.4 - y + 0.3\cos(\frac{2}{3}\pi x)}{2\sqrt{2}\epsilon}\right), & \text{if } (x < 3) \\ \frac{1}{2} + \frac{1}{2}\tanh\left(\frac{0.4 + y + 0.3\cos(2\pi x)}{2\sqrt{2}\epsilon}\right), & \text{others,} \end{cases} \tag{9}$$

$(x, y) \in \Omega$, where $\Omega = (0, 4) \times (0, 1.5)$. Here, $\epsilon_m = mh/[4\sqrt{2}\tanh^{-1}(0.9)]$. We also use two different values of $\lambda_0 = 30$ and $\lambda_0 = 100$. The time evolution of ϕ for $\lambda_0 = 30$ and $\lambda_0 = 100$ are displayed in Fig. 4(a) and (b), respectively.

We observed that tissue grows rapidly in areas with high positive curvature and relatively slowly in areas with high negative curvature. Additionally, when λ_0 is small, the tissue growth is slow as illustrated in Fig. 4(a). However, as λ_0 increases, the rate of tissue growth accelerates, as illustrated in Fig. 4(b).

3.2.3. Effect of α

To examine the effects of other parameters, we investigate the effect of α with the initial condition (9). The parameters $\beta_0 = 0.5$, $T =$

$40\,000\Delta t$, and $\lambda_0 = 30$ are used, and the other parameter values used are the same as in the previous test. We observe the parameter effects for three different values of $\alpha = 0.05$, $\alpha = 0.5$ and 1. Fig. 5 shows the numerical test results for three different α values.

As a result, the effect of α was minimal with small $|\kappa|$. However, with large curvature κ, as shown in Fig. 5, the closer α is to 1, the slower the growth in regions with negative curvature κ and the faster the growth in regions with positive curvature κ.

3.2.4. Comparison test with a real experiment

We investigate the process of tissue growth on different scaffolds and compare it with experimental results by Rumpler et al. [22]. The different scaffolds have triangular pores in the first row, square pores in the second row, and hexagonal pores in the third row. Fig. 6 represents the evolution process up to $T = 30\,000\Delta t$ is divided into $t = 10\,000\Delta t$, $20\,000\Delta t$, and $30\,000\Delta t$ for analysis. The domain is set as $\Omega = (0, 1)\times(0, 1)$, with parameters $h = 0.01$, $\epsilon = \epsilon_5$, $\Delta t = 4\epsilon^2 h^2/(h^2+16\epsilon^2)$, $\lambda_0 = 5$, $\alpha = 0.9$, and $\beta = 1$.

To validate our model, we compare the result of another in vitro experiment with that of our proposed model. Fig. 7(a) shows the in vitro experimental results from Bidan et al. [15]. Overall, tissue grows, but it was observed that the growth rate is higher in convex regions compared to concave regions. The result of our proposed model, using the following parameters, is shown in Fig. 7(b). Here the parameters used are $\lambda_0 = 95$, $\alpha = 0.85$, $\beta_0 = 4$, $h = 0.005$, $\epsilon = \epsilon_{10}$, $\Delta t = 4\epsilon^2 h^2/(h^2 + 16\epsilon^2)$, and $T = 22\,000\Delta t$. As a result, we confirmed that the obtained result closely matches the actual experimental result.

4. Conclusion

In this study, we introduced a novel phase-field model designed to simulate curvature-dependent and surface-limited tissue growth on curved surfaces using an advanced modification of the AC equation. By incorporating non-standard variable mobility and growth terms, our model effectively captures complex growth behaviors. The implementation of an operator splitting method allows for efficient numerical solutions by decomposing the governing equation into several components. The efficacy and robustness of the proposed model are demonstrated through a series of numerical simulations such as synthetic initial conditions and comparisons with real experimental data. These results validated the model's potential for advancing simulations in growth phenomena and provided a valuable tool for further research and practical applications. The numerical tests in the paper validated the performance of a novel phase-field model for tissue growth influenced by curvature. The convergence test confirmed second-order spatial accuracy and first-order temporal accuracy. The impact of the growth parameter λ_0 and curvature sensitivity parameter α was studied, which showed that increased λ_0 accelerates growth, while larger α enhances growth in positively curved regions and suppresses it in negatively curved ones. Qualitative comparisons with experimental results validated the model's ability to simulate realistic growth patterns, particularly the higher growth rate in convex regions. These numerical tests highlighted the model's robustness and efficiency in simulating curvature-dependent tissue growth on curved surfaces. For future research, we plan to investigate three-dimensional tissue growth on complex bio-scaffold surfaces [25,26] using a multi-dimensional AC equation [27].

CRediT authorship contribution statement

Soobin Kwak: Writing – review & editing, Writing – original draft, Visualization, Validation, Software, Methodology, Investigation, Formal analysis, Data curation, Conceptualization. **Yongho Choi:** Writing – review & editing, Writing – original draft, Validation, Methodology, Formal analysis, Conceptualization. **Jian Wang:** Writing – review & editing, Writing – original draft, Validation, Investigation, Formal analysis. **Yunjae Nam:** Writing – review & editing, Writing – original draft, Visualization, Investigation, Data curation. **Junseok Kim:** Writing – review & editing, Writing – original draft, Validation, Supervision, Project administration, Methodology, Investigation, Funding acquisition, Formal analysis, Conceptualization.

Declaration of competing interest

The authors declare that they have no known competing financial interests or personal relationships that could have appeared to influence the work reported in this paper.

Acknowledgment

The corresponding author (J.S. Kim) was supported by the Brain Korea 21 FOUR through the National Research Foundation of Korea funded by the Ministry of Education of Korea. We sincerely thank the reviewers for their valuable comments and constructive suggestions, which have significantly improved the quality of our manuscript.

Data availability

No data was used for the research described in the article.

References

[1] Nelson CM, Jean RP, Tan JL, Liu WF, Sniadecki NJ, Spector AA, Chen CS. Emergent patterns of growth controlled by multicellular form and mechanics. Proc Natl Acad Sci USA 2005;102(33):11594–9. http://dx.doi.org/10.1073/pnas.0502575102.

[2] Pohlmeyer JV, Waters SL, Cummings LJ. Mathematical model of growth factor driven haptotaxis and proliferation in a tissue engineering scaffold. Bull Math Biol 2013;75:393–427. http://dx.doi.org/10.1007/s11538-013-9810-0.

[3] Chanet S, Martin AC. Mechanical force sensing in tissues. Prog Mol Biol Transl Sci 2014;126:317–52. http://dx.doi.org/10.1016/B978-0-12-394624-9.00013-0.

[4] Iwanciw D, Rehm M, Porst M, Goppelt-Struebe M. Induction of connective tissue growth factor by angiotensin II: Integration of signaling pathways. Arterioscler Thromb Vasc Biol 2003;23(10):1782–7. http://dx.doi.org/10.1161/01.ATV.0000092913.60428.E6.

[5] Lanza R, Langer R, Vacanti JP, Atala A. Principles of tissue engineering. Academic Press; 2020.

[6] Khademhosseini A, Vacanti JP, Langer R. Progress in tissue engineering. Sci Am 2009;300(5):64–71, https://www.jstor.org/stable/26001345.

[7] Polo-Corrales L, Latorre-Esteves M, Ramirez-Vick JE. Scaffold design for bone regeneration. J Nanosci Nanotechnol 2014;14(1):15–56. http://dx.doi.org/10.1166/jnn.2014.9127.

[8] Zadpoor AA. Bone tissue regeneration: The role of scaffold geometry. Biomater Sci 2015;3(2):231–45. http://dx.doi.org/10.1039/C4BM00291A.

[9] Huang Q, Qiao Z, Yang H. Maximum bound principle and non-negativity preserving ETD schemes for a phase field model of prostate cancer growth with treatment. Comput Methods Appl Mech Engrg 2024;426:116981. http://dx.doi.org/10.1016/j.cma.2024.116981.

[10] Alotaibi M, Foucher F, Ibrahim M, Saad M. Computational modeling of early-stage breast cancer progression using TPFA method: A numerical investigation. Appl Numer Math 2024;198:236–57. http://dx.doi.org/10.1016/j.apnum.2024.01.010.

[11] López-Agredo JL, Rueda-Gómez DA, Villamizar-Roa ÉJ. Theoretical and numerical analysis of a parabolic system with chemoattraction modeling the growth of glioma cells. Appl Numer Math 2023;186:143–63. http://dx.doi.org/10.1016/j.apnum.2023.01.008.

[12] Han P, Xu W, Zhang H, Wang L. Most probable trajectories in the delayed tumor growth model excited by a multiplicative non-Gaussian noise. Chaos Solitons Fractals 2022;156:111801. http://dx.doi.org/10.1016/j.chaos.2022.111801.

[13] Ghanizadeh M, Shariatpanahi SP, Goliaei B, Rüegg C. Mathematical modeling approach of cancer immunoediting reveals new insights in targeted-therapy and timing plan of cancer treatment. Chaos Solitons Fractals 2021;152:111349. http://dx.doi.org/10.1016/j.chaos.2021.111349.

[14] Wang F, Idrees M, Sohail A. AI-MCMC for the parametric analysis of the hormonal therapy of cancer. Chaos Solitons Fractals 2022;154:111618. http://dx.doi.org/10.1016/j.chaos.2021.111618.

[15] Bidan CM, Kommareddy KP, Rumpler M, Kollmannsberger P, Bréchet YJ, Fratzl P, Dunlop JW. How linear tension converts to curvature: Geometric control of bone tissue growth. PLoS One 2012;7(5):e36336. http://dx.doi.org/10.1371/journal.pone.0036336.

[16] Lee HG, Park J, Yoon S, Lee C, Kim J. Mathematical model and numerical simulation for tissue growth on bioscaffolds. Appl Sci-Basel 2019;9(19):4058. http://dx.doi.org/10.3390/app9194058.
[17] Yang J, Li Y, Lee C, Kim J. Conservative Allen–Cahn equation with a nonstandard variable mobility. Acta Mech 2020;231:561–76. http://dx.doi.org/10.1007/s00707-019-02548-y.
[18] Choi Y, Kim J. Maximum principle preserving and unconditionally stable scheme for a conservative Allen–Cahn equation. Eng Anal Bound Elem 2023;150:111–9. http://dx.doi.org/10.1016/j.enganabound.2023.02.016.
[19] Shen J, Tang T, Yang J. On the maximum principle preserving schemes for the generalized Allen–Cahn equation. Commun Math Sci 2016;14(6):1517–34. http://dx.doi.org/10.4310/CMS.2016.v14.n6.a3.
[20] Xia B, Yu R, Song X, Zhang X, Kim J. An efficient data assimilation algorithm using the Allen–Cahn equation. Eng Anal Bound Elem 2023;155:511–7. http://dx.doi.org/10.1016/j.enganabound.2023.06.029.
[21] Hwang Y, Ham S, Lee C, Lee G, Kang S, Kim J. A simple and efficient numerical method for the Allen–Cahn equation on effective symmetric triangular meshes. Electron Res Arch 2023;31(8):4557–78. http://dx.doi.org/10.3934/era.2023233.
[22] Rumpler M, Woesz A, Dunlop JW, Van Dongen JT, Fratzl P. The effect of geometry on three-dimensional tissue growth. J R Soc Interface 2008;5(27):1173–80. http://dx.doi.org/10.1098/rsif.2008.0064.
[23] Emamjomeh M, Nabati M, Dinmohammadi A. Numerical study of two operator splitting localized radial basis function method for Allen–Cahn problem. Eng Anal Bound Elem 2024;163:126–37. http://dx.doi.org/10.1016/j.enganabound.2024.02.016.
[24] Ham S, Kim J. Stability analysis for a maximum principle preserving explicit scheme of the Allen–Cahn equation. Math Comput Simulation 2023;207:453–65. http://dx.doi.org/10.1016/j.matcom.2023.01.016.
[25] Xia Q, Sun G, Kim J, Li Y. Multi-scale modeling and simulation of additive manufacturing based on fused deposition technique. Phys Fluids 2023;35(3). http://dx.doi.org/10.1063/5.0141316.
[26] Zamani-Gharaghoshi H, Dehghan M, Abbaszadeh M. Numerical solution of Allen–Cahn model on surfaces via an effective method based on generalized moving least squares (GMLS) approximation and the closest point approach. Eng Anal Bound Elem 2023;152:575–81. http://dx.doi.org/10.1016/j.enganabound.2023.04.019.
[27] Hwang Y, Kim I, Kwak S, Ham S, Kim S, Kim J. Unconditionally stable monte carlo simulation for solving the multi-dimensional Allen–Cahn equation. Electron Res Arch 2023;31(8):5104–23. http://dx.doi.org/10.3934/era.2023261.